Journal of Theoretical and Applied Information Technology

www.jatit.org

SPACECRAFT FLYWHEEL HIGH SPEED PM SYNCHRONOUS MOTOR DESIGN (CLASSICAL&GENETIC)

[1]A. EL SHAHAT, [2]A. KEYHANI, [3]H. EL SHEWY

[1]Research Scientist, Mechatronics-Green Energy Lab., Elect. & Comp. Eng. Dept., OSU, USA, 43210

[2]Professor, Director of Mechatronics-Green Energy Lab., Elect. & Comp. Eng. Dept., OSU, USA, 43210

[3]Professor, Department of Electrical Power & Machines Engineering, Zagazig University, Egypt

E-mail: adel.elshahat@ieee.org, ahmed.210@osu.edu, adel2029@yahoo.com

ABSTRACT

High Speed PM Motors are popularly used in Spacecraft flywheel application. So, this paper proposes two different designs: one for classical sizing and the other for genetic one at 50 kW output power with 250 m/s tip speed. These two design trials of High Speed Permanent Magnet Synchronous Motors (HSPMSMs) are simulated with MATLAB, and Genetic Algorithm Toolbox. Then, the two design examples comparisons are introduced in analytical forms with study of machines waveforms, Total Harmonic Distortion (THD) and rotor losses. Finally, the effect of poles number on some sizing parameters and motor characteristics are illustrated in the form of charts with the waveforms. This is done at constant number of slots and phases with number of poles are 4, 6, and 12 at 50 kW output power and tip speeds of 250, 200, 150, and 100m/s.

Keywords: *High Speed, Flywheel, Genetic Algorithm, PM Motors, MATLAB, Spacecraft.*

1. INTRODUCTION

The High Speed PM Synchronous Motor is widely used in Spacecraft and Aircraft applications. In addition, recent technological advances in small generators, Power Electronics, and energy storage devices have provided new opportunities in the field of energy generation [1-3], [8]. So, more attention has been paid to the development of high speed PM machines driven by micro-turbines, as prime movers with local conversion at load points [4]. High speed permanent magnet (PM) motors provide a substantial reduction in size and weight over other types of machines, and they are also higher in power density, since, as the speed of a machine increases, its size decreases for a given output power. Size, weight, and cost are the major factors for successful design. For high-speed applications, the rotor aspect ratio, defined as length-to-diameter, is a critical parameter. Stator core losses may be minimized by using laminated steel in stator construction and by not generating frequencies that are too high. The main applications of PMSM are for power generation as part of renewable energy resources, spacecraft flywheel and main generators for aircraft, etc. [5-14]. The sizing of HSPMSM design must address system topology for good power/volume, low cost, and superior efficiency. The influence of the choice of stator lamination material on iron loss in a high speed, high power, and permanent magnet machine is investigated. We study also the genetic optimum design of high speed PM machines for applications in spacecraft applications or distributed power generation systems [4-17]. Moreover, the high speed PM machine has been widely used in distributed power generation.

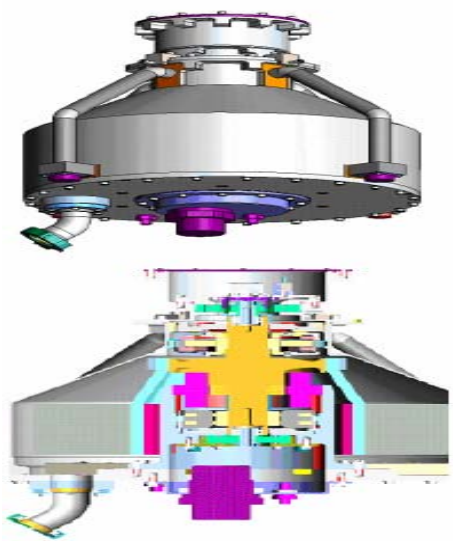

Figure 1: Spacecraft Flywheel [14]

The high speed generator distributed generation system, in comparison with the PM doubly-fed reluctance generator, for the same application, has better electromagnetic properties, and (the PM doubly-fed reluctance machine exhibits better mechanical behavior [25]. Aspects of PM motor technology and the design of brushless PM machines, as introduced in Hanselmann [15] and Hendershot [16], are used in this paper.

2. MACHINE DESIGN PARAMETERS

A. Machine Materials

The rare earth magnets, SmCo and NdFeB, have become popular because of their greater power density, high Coercivity, high flux densities, and the linearity of their demagnetization curves [16] and [18]. NdFeB is preferred because it is cheaper and more readily available. Therefore, NdFeB magnets are selected for use in PMM, with some conservatively assumed values [17]. The rotor is usually built from the same material as the stator for ease of construction, but it can be made of any economical steel, provided it is strong enough for its function [16], [19]. TM19, 29 gauge electrical silicon steel is selected for the PMM because it is economical, its thin laminations minimize power losses due to the circulating eddy current, and because it has a saturation flux density of about 1.8 T [16], [17].

B. Mechanical Design

The stator is an important part of the machine because it serves as the main structural component, it provides the housing for the armature windings, and it completes the flux path for the magnetic circuit. Slotted stators are the traditional stator design and consist of openings around the stator for the armature windings. In this paper, the slots are trapezoidal, but assumed to be approximately rectangular. They contain form-wound windings so that the depression width is the same as the top slot width. Slotting is used because of its advantages, such as the achievement of a narrow air gap length to maximize the flux linkage, the increase in surface contact area between the windings, and a path of low thermal resistance, provided by stator steel for good heat conduction [17]. The initial design of the generator assumes a three-phase machine. Also, a 36 slots machine is chosen for the initial generator design [16]. A general machine mechanical shape is shown in figure 2.

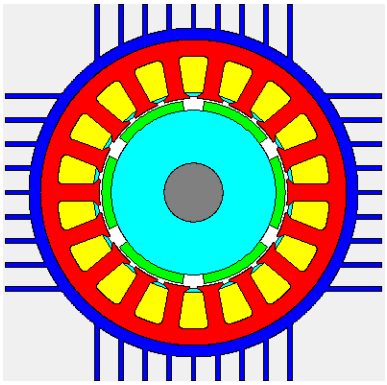

Figure 2: Surface mounted PM machine shape.

The surface mounted permanent magnets in the rotor as shown in figure 2. For high-speed applications, the rotor aspect ratio, defined as length-to-diameter (L/D), is a critical parameter. PM machines offer flexibility in selecting pole sizes, which allows for smaller diameters. A normal L/D ratio for a wound rotor machine is 0.5 – 1.0, compared to 1 – 3 for a PM machine [20]. So, here it is selected to be 2.5. The rotor radius and rotational speed also determine the tip speed of the machine, which is the surface velocity of the rotor.

$$v_{tip} = r\omega_m \tag{1}$$

ω_m: angular speed (rad/sec); r: rotor radius (m)

C. Number of Poles and Magnets Pole Design

An even number of poles is always used, here P = 3, because this provides a balanced rotational design. Assuming a constant mechanical rotation speed, electrical frequency is given as.

$$N(2P) = 120\, f \tag{2}$$

N = speed (rpm); P = pole pairs; f = frequency

However, as the frequency increases, higher stator losses result because core losses are proportional to frequency squared. In addition, as the pole number gets larger, the number of slots per pole per phase decreases and can cause the voltage waveforms to become less sinusoidal so all factors must be considered. The pole arc of the magnets can also be varied. Magnets seldom span the full pole pitch because the flux at the transition between north and south poles leaks between poles without linking the coils in the stator. The gaps between the poles usually contain non – magnet pieces, such as soft iron, so that no flux crosses over the air gap

between magnets. All full pole arc is α_{me} = 180 ^{o}E and produces a full voltage waveform but has increased harmonic content. As the pole arc is reduced (up to 20 – 30 %) and those areas are filled in with soft – iron pieces, the resulting flux waveform is more sinusoidal and has fewer harmonics and therefore lower rotor losses. The magnet poles are sometimes skewed to reduce cogging torque and smooth out variations in air gap reluctance, flux, and voltage waveforms. Skewing of magnets occurs axially along the length of the rotor to provide a constant rotational torque and prevent pole pieces from exactly lining up with stator teeth. Magnet poles skew factor is selected to reduce cogging torque and smooth out variations in air gap reluctance, flux, and voltage waveforms.

$$k_{sn} = \frac{\sin(n\theta_s)}{\frac{\theta_s}{2}} \quad (3)$$

where θs: Skew angle, rad E; n: Harmonic number

D. Magnetic Dimensions

The magnetic dimensions that affect a PM machine are air gap and magnet height. The air gap flux density (B_g) can be represented by Eq. 4. The radial air gap is made as small as possible to maximize the air gap flux density, minimize the flux leakage, and to produce a lower reluctance value.

$$B_g = \frac{h_m}{h_m + g} B_r \quad (4)$$

where h_m: Magnet height (mm); g: Air gap (mm); B_r: Magnet Remnant Flux Density (T)

Magnets losses are reduced, using smaller magnets. For uniform magnetic fields, the magnet height is usually larger than the air gap, by a factor 5 – 10.

E. Slots per Pole, Per Phase

Three-phase machines are typically used in this paper as the standard choice for most motors and generators. Another important design parameter is the number of slots per pole, per phase (m), as in Eq. 5.

$$m = \frac{N_s}{2 * P * q} \quad (5)$$

Varying the number of slots/pole/phase is used to produce a more sinusoidal voltage waveform and reduce machine harmonics.

F. Stator Windings

The pitch of a winding (α) refers to the angular displacement between the sides of a coil. The breadth of a stator winding results from the coils occupying a distribution of slots within a phase belt. In smaller machines, coils are composed of round insulated wires that are placed in the stator slot, along with insulation material. A slot fill factor (λ_s) is used to determine how much of the slot's cross-sectional area is occupied by winding material, as in Eq. 6.

$$\lambda_s = \frac{Winding \quad Area}{Total \quad Slot \quad Area} \quad (6)$$

Typically, machines contain two coils sides per slot, making the winding a double-layer design [16]. Overall, slot fill factors vary in value from 0.3 – 0.7, depending on the number and size of the conductors in the slots, as well as the amount of labor utilized. In this paper, a slot fill factor of 0.5 is assumed. Almost all machines use series, wye – connected windings because they provide the safest alternative. Therefore, wye series connected windings are selected for use in the designs in this study.

G. Machine Calculated Parameters

Each phase of the machine is modeled, as shown in Fig. 3.

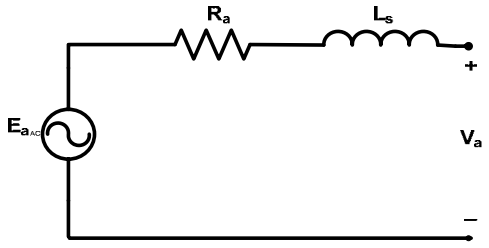

Figure 3: A Per Phase electrical model.

where: R_a: Armature resistance; L_s: Synchronous inductance; E_a: Back e.m.f voltage and V_a: Terminal voltage.

H. Winding Resistances

Resistance of copper phase windings is calculated in Eq. 7

$$R_a = \frac{l}{\sigma * A_{ac}} \quad (7)$$

where l: length of conductor; σ : winding conductivity; A_{ac}: winding cross – sectional area

$$A_{ac} = \frac{A_s * \lambda_s}{2 * N_C} \quad (8)$$

where A_s: slot Area, N_c: turns per coil

But the above stator resistance equation may be used as in low frequencies applications, so it has to be developed. Since the machine rotates at high

speed, and high frequency and so the skin depth may be affected. In conductors that carry high frequency currents, skin effect can become an issue and affect the operation of the machine. Skin effect is caused by eddy currents in the windings themselves due to the changing magnetic field. These eddy currents force the current flowing in the conductor to crowd to the outer edges of the conductor. This in turn causes the current to flow through a smaller cross – sectional area and increase the resistance of the conductor. It is well known that, when conductive material is exposed to an ac magnetic field, eddy currents are induced in the material in accordance with Lenz's law. The power loss resulting from eddy currents which can be induced in the slot conductors appears as an increased resistance in the winding. To understand this phenomenon, let us consider a rectangular conductor as shown in fig. 4. The average eddy current loss in the conductor due to a sinusoidal magnetic field in the y direction is given approximately by Hanselman [15].

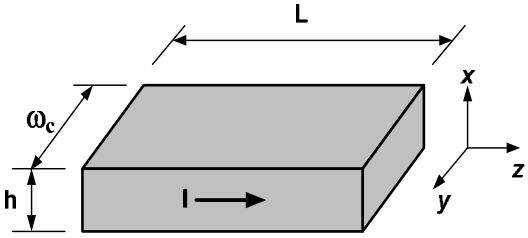

Figure4: Rectangular conductor geometry

$$P_{ec} = \frac{1}{12}\sigma L \omega_c h^3 \omega^2 u_0^2 H_m^2 \quad (9)$$

where H_m: the turn field intensity value; u_0: permeability of free space.

Since skin depth is defined as

$$\delta = \sqrt{\frac{2}{\omega u_0 \sigma}} \quad (10)$$

Equation (9) can be written as

$$P_{ec} = \frac{L \omega_c h^3}{6\sigma\delta^4} H_m^2 \quad (11)$$

Using this expression it is possible to compute the ac resistance of the slot conductors. If the slot conductors are distributed uniformly in the slot, and substituting the field intensity into eq. (11) and summing over all ns conductors gives a total slot eddy current loss of

$$P_e = (\frac{d_s L h^2 n_s^2}{9\sigma\delta^4 \omega_s}) I^2 \quad (12)$$

where I is the rms conductor current; ω_s: Slot width(m); d_s: Slot depth(m)

The slot resistance of a single slot containing ns conductors connected in series is

$$R_{sl} = \frac{\rho n_s^2 L}{k_{cp} \omega_s d_s} \quad (13)$$

where L: the slot length; k_{cp}: the conductor packing factor, is the ratio of cross sectional area occupied by conductors to the entire slot area and ρ: electrical resistivity (Ω.m).

Using eq. (13), the total slot resistance can be written as

$$R_{st} = R_{sl} + R_{ec} = R_{sl}(1 + \Delta_e) \quad (14)$$

In this equation, $\Delta e = R_{ec}/R_{sl}$ is the frequency-dependent term. Using eq. (13) and eq. (12), this term simplifies to

$$\Delta_e \equiv \frac{R_{ec}}{R_{sl}} = \frac{1}{9}(\frac{d_s}{\delta})^2 (\frac{h}{\delta})^2 \quad (15)$$

This result shows that the resistance increases not only as a function of the ratio of the conductor height to the skin depth but also as a function of the slot depth to the skin depth. Thus, to minimize ac losses, it is desirable to minimize the slot depth as well as the conductor dimension. For a fixed slot cross-sectional area, this implies that a wide but shallow slot is best.

I. Winding and Magnet Factors

Winding are short-pitched and have breadth associated with them. To account for these effects, a winding factor (kw) is utilized, as in Equation 16.

$$k_{wn} = k_{pn} * k_{bn} \quad (16)$$

Short-pitching is an important means for eliminating harmonics and improving the power quality of the machine. The pitch factor is shown in Equation 17.

$$k_{pn} = \sin(\frac{n * \alpha}{2}) * \sin(\frac{n * \pi}{2}) \quad (17)$$

The breadth factor explains the effect of the windings occupying a distribution or range of slots within a phase belt. The breadth factor is derived in Equation 18.

$$k_{bn} = \frac{\sin(\frac{n * m * \gamma}{2})}{m * \sin(\frac{n * \gamma}{2})} \quad (18)$$

where m: slots per pole per phase; γ: coil electrical angle

The magnetic flux factor equation [15], for the slotted stator and surface magnet configuration is shown in Equation 19.

$$k_{gn} = \frac{R_i^{np-1}}{R_s^{2np} - R_i^{2np}} * [(\frac{np}{np+1}) * (R_2^{np+1} - R_1^{np+1}) + \frac{np}{np-1} * R_s^{2np} * (R_1^{1-np} - R_2^{1-np})] \quad (19)$$

where R_s: outer magnetic boundary, R_2: outer boundary of magnet; R_i: inner magnetic boundary, R_1: inner boundary of magnet

J. Flux and Voltage

For useful voltage, only the fundamental components are used to determine the internal voltage (back e.m.f) of the generator, as shown in Equations 20, 21, and 22.

$$E_a = \omega_0 \lambda \quad (20)$$

$$\lambda = \frac{2 * R_s * L_{st} * N_a * k_w * k_s * B_1}{P} \quad (21)$$

$$B_1 = \frac{4}{\pi} * B_g * k_g * \sin(\frac{P\theta_m}{2}) \quad (22)$$

where θ_m: magnet physical angle

$$B_g = \frac{k_l C_\phi}{1 + k_r * \frac{u_{rec}}{PC}} * B_r \quad (23)$$

u_{rec}: recoil permeability; B_r: remnant flux density

$$PC = \frac{h_m}{g_e * C_\phi} \quad (24)$$

where PC: permeance coefficient; C_Φ: flux concentration factor (Am/Ag)

$$N_a = 2 * P * N_c \quad (25)$$

where N_c : Turns per coil; N_a : Number of armature turns (each slot has 2 half coils)

$$\tau_s = w_s + w_t ; g_e = k_c * g \quad (26)$$

where g_e: eff. air gap; w_s: average slot width; w_t: tooth width

Here, a leakage factor (Kl ≅ 0.95) and a reluctance factor (Kr ≅1.05) are both used for surface magnets. The presence of the slots in the stator also affects the air gap flux density because of the difference in permeance caused by the slots. Carter's coefficient (k_c) is used to account for this effect [15].

$$k_c = [1 - \frac{1}{\frac{\tau_s}{w_s} * (5 * \frac{g}{w_s} + 1)}]^{-1} \quad (27)$$

The terminal voltage (V_a) is calculated from the internal voltage (E_a), and the synchronous reactance voltage drop. The armature resistance is usually ignored because it is much smaller than synchronous reactance. The voltage is found as a relation in output power (P_{wr}), e.m.f, and reactance from the resulting quadratic equation.

$$V_a = \sqrt{\frac{BB + \sqrt{BB^2 + 4CC}}{2}} \quad (28)$$

$$BB = E_a^{\ 2}; \; CC = X_s^{\ 2} \frac{P_{input}^{\ 2}}{9}$$

K. Machine Inductances

In a slotted PM machine, there are three distinct components of inductance: the largest, air gap inductance slot leakage inductance, and the smallest, end-turn inductance. The total inductance for the phase is the sum of the three inductances, ignoring other small factors.

$$L_s = L_{ag} + L_{slot} + L_e; \quad X_s = \omega_0 * L_s \quad (29)$$

The air gap inductance is given by Eq. 30.

$$L_{ag} = \frac{\lambda}{i} = \frac{q}{2} * \frac{4}{n\pi} * \frac{u_0 * R_s * L_{st} * N_a^{\ 2} * k_{wn}^{\ 2}}{n^2 * P^2 * (g + h_m)} \quad (30)$$

The slot leakage inductance is presented in Eq. 31. Assume the slot is rectangular with slot depressions, as in Fig. 2, and assume (m) slots per pole per phase, with a standard double layer winding.

$$L_{slot} = L_{as} - L_{am}; (3\,phase) \quad (31)$$

$$L_{am} = 2 * P * L_{st} * Perm * N_{sp} * N_c^{\ 2} \quad (32)$$

$$L_{as} = 2*P*L_{st}*Perm*[4*N_c^{\ 2}(m - N_{sp}) + 2*N_{sp}*N_c^{\ 2}] \quad (33)$$

A slot permeance per unit length is shown in Equation 34.

$$Perm = \frac{1}{3} * \frac{h_s}{w_{st}} + \frac{h_d}{w_d} \quad (34)$$

The end turn inductance is introduced in Eq. 35, assuming the end turns are semi-circular, with a radius equal to one-half the mean coil pitch.

$$L_e = \frac{u_0 * N_c * {N_a}^2 * \tau_s}{2} * \ln(\frac{\tau_s * \pi}{\sqrt{2 * A_s}}) \quad (35)$$

L. Basic Losses

Losses in a machine consist of core losses, conductor losses, friction and windage losses, and rotor losses. Rotor losses will be discussed later. Stator core losses, per weight, can be greater than normal in machines because of higher frequencies. These losses are minimized by using laminated steel in stator construction and by not generating frequencies that are too high. Core losses consist of hysteresis and eddy current losses. The best way to approximate core losses is to use empirical loss data. An exponential curve fitting is applied to the empirical data for M-19, 29 gauge material, in order to obtain an equation for estimating core losses, as in Equation 36, with constant values in [22].

$$P_C = P_0 * (\frac{B}{B_0})^{\varepsilon B} * (\frac{f}{f_0})^{\varepsilon f} \quad (36)$$

where P_0: Base power; B_0: Base flux density; ε_B: Flux density exponent; f_0: Base frequency; ε_f: Frequency exponent

The above commonly used equation considering hysteresis and eddy-current loss is not completely satisfactory, because the measured iron loss is much higher than theoretically calculated. This is so because it assumes a homogenous magnetization of the laminations, which is not a valid representation of what happens during the magnetization process. The loss caused by the movements of the magnetic domain walls is higher than the loss calculated with the commonly used equation. The difference between measured and calculated loss is called the excess loss or the anomalous loss. Sometimes, this anomalous or excess loss is considered as a third contribution to the iron loss. Great efforts have been made to calculate this excess loss, because of the complexity of the domain patterns. For reasons mentioned before, it is useful to represent the core loss by core loss resistance, which is placed in equivalent circuit. The core loss resistance is connected across the voltage V_a. Therefore, the power dissipated in this resistance is [26-34].

$$P_{R_c}(\omega) = \frac{V_a^2}{R_c} \quad (37)$$

$$R_c(\omega) = \frac{3\pi^2 {L_{st}}^2 N_a^2 \sqrt{\omega}}{8 c_{Fe} k_{Fe} (\frac{1}{\omega_0})^{1.5} (\frac{1}{B_0})^2 \{m_{st} (\frac{p\beta_{slot}}{b_{st}})^2 + m_{sy} (\frac{1}{h_{sy}})^2\}} \quad (38)$$

where R_c: core resistance, c_{Fe}: correction factor for iron loss calculation, b_{st}: stator tooth width, k_{Fe}: specific iron loss, m_{st}: stator teeth mass, βslot: slot angle, h_{sy}: stator yoke height

When this core loss resistance is depicted in an equivalent circuit, it should be noted that the resistance is frequency dependent.

The conductor losses are found, using Equation 39.

$$P_a = q * I_a^2 * R_a \quad (39)$$

For rotors operating at high speed, the friction and windage in air can cause losses which result in inefficiency and heat production. These losses are calculated, using the power necessary to overcome the drag resistance of a rotating cylinder, as given by Eq. 40 [23].

$$P_{wind} = C_f * \pi * \rho_{air} * \omega^3 * R^4 * L_{st} \quad (40)$$

The coefficient of friction can be approximated by Eq. 41.

$$C_f \cong 0.0725 * R_{ey}^{-0.20} \quad (41)$$

where Rey: Reynold's Number

M. Classical Sizing

For the basic sizing calculations, an air-cooled generator is assumed with 10 psi [16], [24]. The machine power equation is utilized to derive the rotor radius and stack length of the machine, as in Equation 42.

$$P_{wr} = 2 * \pi * r * L_{st} * v_{tip} * \tau \quad (42)$$

where r : rotor radius; L_{st} : stack length; τ : shear stress (psi)

The L/D ratio is substituted for L_{st}. Using shear stress, rotor tip speed, and machine power rating range, the power equation is calculated to obtain rotor radius and stack length, while matching the desired rotational speed of the machine with a L/D ratio equal to 2.5, as supposed here. Using a pole pair value of 3, a slot height of 10 mm, and a slot fill fraction of 0.5, the frequency is found. Once the basic sizing of the machine is complete, in-depth analysis is conducted to obtain the overall performance. Using the equations presented in previous sections, all the detailed parameters can be obtained. The lengths, volumes, masses, and overall

generator parameters are calculated, using basic geometric equations and relationships. A 15% service mass fraction is added to the total mass estimate to account for the additional services associated with machines cooling [17], [24]. Once the mass of each of the stator parts is known, core losses are estimated in accordance with them. The calculation of lengths, volumes, and weights are presented. The mass of armature conductors, core mass, magnet mass, and shaft mass are calculated to give the total mass value. Finally, stator resistance, terminal voltage, current, loss types, input power, and efficiency are calculated.

3. ANALYTICAL MODEL

This part presents the study of rotor losses caused by stator winding time and space harmonics slot space harmonics.

A. Rotational Stress and Retaining Sleeve

Since the PM motor is spinning at high speed, the rotor and permanent magnets are subjected to extremely high centrifugal forces. These forces can cause significant amounts of damage if the magnets and rotor are not properly restrained. The rotational components can be strengthened by enclosing them in a retaining sleeve/can which also increases the air gap length. The centrifugal force on the magnets due to the rotor spinning is calculated in Eq. (43)

$$F_{cen} = \frac{M_m . v_{mag}^2}{R + h_m} \tag{43}$$

where M_m: mass of magnets; v_{mag}: velocity of magnets

Using the inner surface area of the retaining sleeve, this force is converted to an outward pressure. Treating the retaining sleeve as a thin-walled vessel, the loop stress felt by the sleeve is determined as shown in Eq. (44)

$$\sum_{vert} F_v = -2.\sigma_c .h.L + \int_0^{\pi} P.r.L.\sin(\theta).L.d\theta = 0$$

$$\sigma_C = \frac{P.r}{h} \tag{44}$$

A suitable safety factor is applied to the hoop stress to get a final SF stress for the retaining sleeve. The retaining sleeve can be made from many different types of materials including metal alloys and composites. A disadvantage of a metallic sleeve is eddy currents are induced in the sleeve by variations in the flux density caused by the stator slots [40 – 42]. From our calculations with various materials with our initial gap length; it is not sufficient once the retaining sleeve is considered (since the air gap dimension includes the retaining sleeve thickness). So, the machine must therefore be revised to allow for the retaining can and redesigned taking the retaining sleeve and hoop stress limits into consideration. But, this updated machine will be bigger one with a much larger air gap, greater magnet height, lower B_g, lower voltage, and higher current density. So, we prefer her not to use the sleeve and keep the smaller machine with restriction to the manufacturer to firm the magnet rigidly.

B. Rotor Losses

1) Model for Time Harmonics & Winding Space Harmonics

The permanent magnets used in high-speed motors are electrically conductive and therefore support eddy currents. The retaining sleeves are sometimes made from electrically conductive material that also can carry eddy currents. These eddy currents are primarily caused by fluctuations in the magnetic flux density produced by time and space harmonics of the winding currents. The currents produce losses which can potentially cause excessive heating or demagnetization of the permanent magnets. An analytical model is developed using the winding and current harmonics and the surface impedance to estimate the rotor losses. Fig. 5 shows the PM motor geometry "flattened out" into rectilinear coordinates. This is an accurate representation provided the dimensions are on a radial scale that is much smaller than the radius of the machine so that curvature is not important [40-42]. The direction of rotation is in the positive x-direction, the radial direction is y, and the armature current flows in the axial dimension, z.

The following assumptions are made in developing the rotor analytical loss model:

- Layers of material extend to ± infinity in the ± x direction.
- Layers effectively extend to negative infinity in the negative y direction.
- Motion/rotation is in the + x direction.
- The physical constants of the layers are homogeneous, isentropic, and linear.
- The ferromagnetic material does not saturate.
- The machine is long axially so magnetic variations in the z direction are ignored (H and B only vary in x, y directions).
- All currents flow in the z direction.

- The rotor and stator are constructed of laminated steel so their conductivity in the z direction is negligible.
- The time and space variations are approximately sinusoidal.
- Flux density at y = infinity is zero.
- A traveling flux wave harmonic can be represented by an equivalent current sheet (K_z) on the surface of the stator.
- The normal component of the flux density is continuous at all interfaces.
- The tangential component of the flux density is continuous at all interfaces except at the stator/air gap where it is increased by the current sheet density.
- The magnetic flux density crossing the air gap and the magnets is perpendicular.
- The effect of magnet eddy currents on the magnetic flux density is negligible – this is accurate below 10 kHz [43].
- The magnet flux density is constant over the magnet breadth

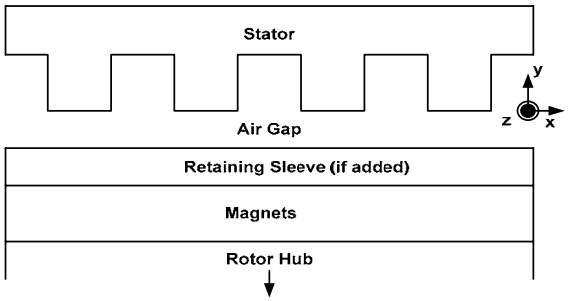

Figure 5: General Magnet Loss Model

$$-<S_y>=-\frac{1}{2}\left|k_z\right|^2.\mathrm{Re}(Z_s)$$
$$-<S_y>=-\frac{1}{2}\left|H_x\right|^2.\mathrm{Re}(\frac{E_z}{H_x}) \quad (45)$$
$$-<S_y>=-\frac{1}{2}\mathrm{Re}(E_z.\bar{H}_x)$$

Eq. (45) yields the power dissipated at the stator surface. This is the correct result for the rotor because there is no mechanism for dissipating power between the stator and rotor. The power estimated by Poynting's theorem flows directly from the stator to the rotor [42].

$$z_s=\frac{\omega_n}{k_n}.u_0.\sigma \quad (46)$$

$$z_s=\frac{E_{surf}}{k_{surf}}=\frac{E_z}{-H_x}=\frac{\frac{-\omega_n}{k_n}.u_0.H_y}{-H_x}$$

Surface impedance (Z_s) is the ratio of the z-directed electric field to the z-directed current, Eq. (46). A final expression for the top surface coefficient is determined Eq. (47), and it is applicable to any uniform region.

$$\alpha_t=j.\frac{k}{\gamma}.[\frac{j.\frac{k}{\gamma}.\sinh(\gamma h)+\alpha_b.\cosh(\gamma h)}{j.\frac{k}{\gamma}.\cosh(\gamma h)+\alpha_b.\sinh(\gamma h)}] \quad (47)$$

If the region being examined is positioned on top of a ferromagnetic surface, such as the magnets on the steel rotor shaft, the boundary condition at the bottom of the layer ($\alpha b \to \infty$ as $Hx \to 0$) produces Eq. (48).

$$\alpha_t=j.\frac{k}{\gamma}.\coth(\gamma h) \quad (48)$$

In the case of the air gap where the conductivity is zero, Eq. (47) reduces to Eq. (49).

$$\alpha_t=j.[\frac{j.\sinh(\gamma h)+\alpha_b.\cosh(\gamma h)}{j.\cosh(\gamma h)+\alpha_b.\sinh(\gamma h)}] \quad (49)$$

At the top of the layer (y=h), the surface coefficient is shown in Eq. (50).

$$\alpha_t=j.\frac{k}{\gamma}.(\frac{\frac{H_p}{H_n}.e^{\gamma h}-.e^{-\gamma h}}{\frac{H_p}{H_n}.e^{\gamma h}+.e^{-\gamma h}}) \quad (50)$$

A surface coefficient is defined as the ratio of the y-directed to x-directed magnetic field amplitude (α = HY/HX). At the bottom of the layer where y = 0, the surface coefficient is given by Eq. (51).

$$\alpha_b=j.\frac{k}{\gamma}.(\frac{\frac{H_p}{H_n}-1}{\frac{H_p}{H_n}+1}) \quad (51)$$

$$H_x=\mathrm{Re}[H_X.e^{j.(\omega t-kx)}] \quad (52)$$
$$H_y=\mathrm{Re}[H_Y.e^{j.(\omega t-kx)}]$$

Solving for the magnetic flux densities and magnetic fields produces Eq. (52), also all these analyses are done with the aid of Faraday's Law, Maxwell's Law and Ampere Law.

In order to calculate the rotor losses, the above analytical model is applied to the geometry in fig. 5. For this model, the stator is assumed to be a smooth surface without slots because the slot effects are consider later. The first step is calculating the surface coefficient at the bottom of the magnet layer. It is assumed that this is formed by the highly permeable rotor shaft below the magnets. This assumption allows the surface coefficient at the top of the magnet layer to be calculated also.

2) Model for Stator Slot Effects

The stator slots cause variations in the magnetic field which losses in the retaining sleeve and magnets of the rotor. Accurate calculation of the losses in the retaining sleeve is extremely difficult. Several different methods have been developed and in this paper, the technique from reference [16] is employed. As the rotor spins past the slot openings of the stator, the air gap flux density undergoes modulation due to the change in reluctance. The dip in B_g (shown in fig. 6) travels along the B-waveform which is otherwise moving synchronously with the rotor.

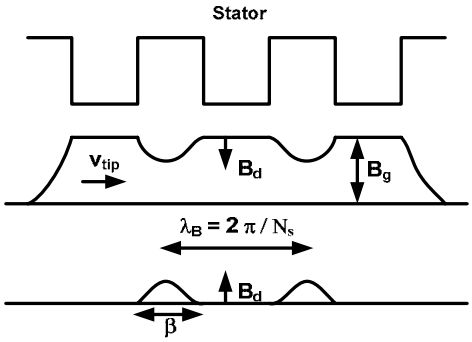

Figure 6: Flux Density Variation

The rotation of the rotor generates an E-field in the sleeve and a subsequent axial current density J=E/p. When this current density is integrated over the volume of the can, the average loss per unit area is determined Eq. (53) [16].

$$w = \frac{\pi^2}{3600}.\frac{[B.N.(R+hm)]^2.t}{\rho} \qquad B = \frac{B_d}{\sqrt{2}}.\sqrt{\frac{\beta}{\lambda_B}} \tag{53}$$

It is evident from Eq. (53) that as the slot width increases, the width of the flux density dip (β) gets larger causing the sleeve losses to increase. The above equation only considers eddy currents flowing in the axial direction but there are also circumferential components. These portions are accounted for using a factor K_s as shown in Eq. (54) where the total can losses are determined [16].

$$P_{can} = K_s.w.A \qquad A = \pi.2.(R+h_m).L_{st} \qquad K_s = 1 - \frac{\tanh[\frac{\rho.L_{st}}{2.(R+h_m)}]}{[\frac{\rho.L_{st}}{2.(R+h_m)}]} \tag{54}$$

One way to reduce the retaining losses is to split the sleeve cylinder (if used) into separate rings. The magnet losses are calculated using methods similar to Eq. (53) and Eq. (54) assuming that the eddy current flow in the top 10% of the magnet volume.

A. Machine THD

HSPM motor produces back EMF waveforms that are dependent on a number of factors as discussed before. The goal is to produce a voltage waveform that closely resembles a sinusoidal waveform with a low total harmonics distortion (THD) because this results in minimal harmonic content which reduces losses in the machine. THD is a measure of the distortion in a waveform caused by undesirable frequency components. It is calculated as shown in Eq. (55).

$$THD = \sqrt{\frac{\sum_{(n\neq 1)} E_{anrms}^2}{E_{a1rms}^2}} \tag{55}$$

The back EMF waveforms are generated using the below eq.s

$$B(\theta) = \sum_{\substack{n=1 \\ n\_odd}}^{\infty} B_n.\sin(np\theta) \qquad B_n = \frac{4}{n\pi}.B_g.k_{gn}.\sin(\frac{np\theta_m}{2}).\sin(\frac{n\pi}{2}) \tag{56}$$

θm: magnet physical angle; n: harmonic number

$$\lambda(\theta) = \sum_{\substack{n=1 \\ n\_odd}}^{\infty} \lambda_n.\sin(np\theta) \qquad \lambda_n = \frac{2.R_s.L_{st}.N_a.B_n.k_{wn}.k_{sn}}{p} \tag{57}$$

$$E_a = \sum_{\substack{n=1 \\ n\_odd}}^{\infty} v_n.\sin(np\theta) \qquad v_n = \frac{d}{dt}\lambda_n = \omega_0\lambda_n \tag{58}$$

4. GENETIC HSPMSM SIZING

The genetic algorithm is a method, based on the idea of natural selection, the process that drives biological evolution, which is used here in solving both constrained and unconstrained optimization problems. At each stage of development, the genetic algorithm selects "individuals," at random, from the current "population" to be "parents," and uses them to produce the "children" of the next generation. In this way, the genetic algorithm repeatedly modifies a population of individual solutions. Over successive generations, the population "evolves" towards an optimal solution. We can apply the genetic algorithm to solve a variety of optimization problems that are not well-suited for standard optimization algorithms, including problems in which the objective function is discontinuous, non-differential, stochastic, or highly nonlinear.

A. How the Genetic Algorithm Works.

The following outline summarizes how the GA works:

1. The algorithm begins by creating a random initial population.
2. The algorithm then creates a sequence of new populations. At each step, the algorithm uses the individuals in the current generation to create the next population. To create the new population, the algorithm performs the following steps:

a. It scores each member of the current population by computing its fitness value.

b. It scales raw fitness scores to convert them into a more usable range of values.

c. It selects members, called "parents," based on their fitness.

d. It designates some individuals in the current population with lower levels of fitness as "elite." These elite individuals are passed to the next population.

e. It produces children from the parents. Children are produced either by random changes to a single parent mutation, or by the combination of the vector entries of a pair of parents' crossover.

f. It replaces the current population with the children, to form the next generation.

3. It stops when one of the stopping criteria is met.

B. Description of the Non-Linear Constraint Solver

The genetic algorithm uses the Augmented Lagrangian Genetic Algorithm (ALGA) to solve non-linear constraint problems. The optimization problem solved by the ALGA algorithm is min x f (x), such that

$$\begin{gathered} c_i(x) \le 0,\ i = 1 \ldots m; \\ c_{eqi}(x) = 0,\ i = m+1 \ldots m_t \\ A \cdot x \le b;\ A_{eq} \cdot x = b_{eq} \\ lb \le x \le ub, \end{gathered} \tag{59}$$

where c (x) represents the non-linear inequality constraints, c_{eq} (x) represents the equality constraints, m is the number of non-linear inequality constraints, and m_t is the total number of non-linear constraints.

The Augmented Lagrangian Genetic Algorithm (ALGA) attempts to solve a non-linear optimization problem with non-linear constraints, linear constraints, and bounds. In this approach, bounds and linear constraints are handled separately from non-linear constraints. A sub-problem is formulated by combining the fitness function and non-linear constraint function, using the Lagrangian and the penalty parameters. A sequence of such optimization problems are approximately minimized, using the genetic algorithm, such that the linear constraints and bounds are satisfied. A sub - problem formulation is defined as

$$\Theta(x,\lambda,s,\rho) = f(x) - \sum_{i=1}^{m} \lambda_i s_i \log(s_i - c_i(x)) + \sum_{i=m+1}^{mt} \lambda_i c_i(x) + \frac{\rho}{2} \sum_{i=m+1}^{mt} c_i(x)^2 \tag{60}$$

where the components λ_i of the vector (λ) are nonnegative and are known as Lagrange multiplier estimates. The elements s_i of the vector (s) are non – negative shifts, and ρ is the positive penalty parameter.

The genetic algorithm minimizes a sequence of the sub-problem, which is an approximation of the original problem. When the sub-problem is minimized to a required accuracy and satisfies feasibility conditions, the Lagrangian estimates are updated. Otherwise, the penalty parameter is increased by a penalty factor. This results in a new sub-problem formulation and minimization problem. These steps are repeated until the stopping criteria are met. For a complete description of the algorithm, see [38] and [39].

C. Efficiency Maximizer Genetic Sizing

The optimization variables here are; that is, x1, x2, and x3 are the L/D ratio, the rotor radius, and the rotor stack length, respectively. The efficiency function is implemented in the form of m. file. After that, using the genetic algorithm, with the previous technique, to maximize the function and generate the desired variables for this maximization or by more accurate word by optimizing this function with a simple constraints that are [1 0 0] as lower limit, and [3 1 1] as upper limit. Using these optimizing variables, we can deliver all the detailed variables for the desired HSPMSM, at maximum

efficiency. Also, it is important to adjust all options in the Genetic GUI in a proper manner, especially the mutation function, population, selection, and stopping criteria.

$$\eta = \frac{P_{out}}{P_{input}} \quad (61)$$

$$P_{input} = P_{Total\_Losses} + P_{out} \quad (62)$$

5. ANALYTICAL CLASSICAL EXAMPLE

Table 1: Complete Classical Analytical Model

HFPM Machine Design, Surface Magnet, Slotted Stator
Machine Size: Machine Dia.= 0.0885 m; Machine Length= 0.0803 m Rotor Radius= 0.0096 m; Active Length = 0.0480 m Slot Avg Width= 2.3568mm; Slot Height = 10.0000mm Back Iron Thick = 2.2417mm; Tooth Width = 2.7932mm
Machine Ratings: Power Rating= 50.0000kw; Speed = 248487.7553RPM Va (RMS) = 916.4499V; Current = 19.7172A Ea (RMS) = 916.4179V; Arm Resistance = 0.01015ohm Synch React.= 0.3884ohm; Syn Inductance = 0.0050mH Tip Speed = 250.0000m/s; Efficiency = 0.9222 Phases = 3.0000; Frequency = 12424.3878Hz
Stator Parameters: Number of Slots= 36; Num Arm Turns = 12.0000mH Breadth Factor = 0.9659; Pitch Factor = 0.9659 Tooth Flux Dens= 1.7262T; Back Iron Dens = 1.2330mH; Slots/pole/phase = 2.0000
Rotor Parameters: Magnet Height= 20 mm; Magnet Angle = 50 degm Air gap = 2.0000mm ; Pole Pairs = 3.0000 Magnet Remanence = 1.2T ; Air Gap Bg = 0.8631mH Magnet Factor = 1.3959; Skew Factor = 0.9886
Machine Losses: Core Loss = 3.9611kw; Armature Loss = 0.0118kw Windage Loss = 0.2465kw; Rotor Loss = TBD kw
Machine Weights: Core = 0.6056kg Shaft = 0.1073kg Magnet = 0.3649kg Armature = 0.5644kg Services = 0.2463kg Total = 1.8885kg

Table 2: Rotor Losses Caused by Harmonics

Time Harmonic Losses = 0.6610 kw Space Harmonic Losses = 0.0406 kw Total Losses = 0.7017 kw

Magnet Loss = 0.1036 kw; THD = 9.6899

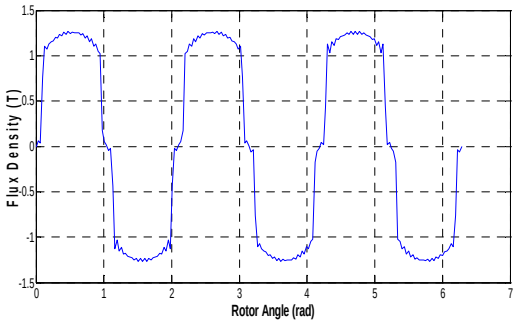

Fig.7: Flux Density Waveform for 50 kW; 250 m/s

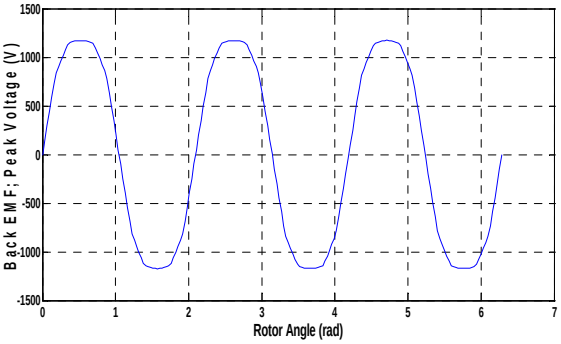

Fig. 8: EMF Waveform for 50 kW and 250 m/s

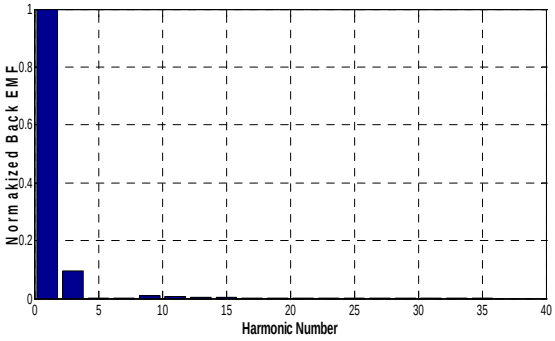

Fig. 9: Harmonic Cont. (9.6899 %) 50 kW; 250 m/s

6. MAX. EFF. GENETIC EXAMPLE

Table.3: Complete Max. Eff. Analytical Model

HFPM Machine Design
Machine Size: Machine Dia. = 0.1023 m; Machine Length = 0.0676 m Rotor Radius = 0.0152 m; Active Length = 0.0304 m Slot Avg Width = 2.8449mm; Slot Height = 10.0000mm Back Iron Thick= 3.5467mm; Tooth Width = 3.2812mm
Machine Ratings: Power Rating= 50.0000kw; Speed = 157060.7991RPM Va (RMS) = 408.4017V; Current = 42.2661A Ea (RMS) = 408.3519V; Arm Resistance = 0.00828ohm

Synch React.= 0.1508ohm; Syn Inductance = 0.0031mH Tip Speed = 250.0000m/s; Efficiency = 0.9648 Phases = 3.0000; Frequency = 7853.0400Hz
Stator Parameters: Number of Slots = 36; Num Arm Turns = 12.0000mH Breadth Factor = 0.9659; Pitch Factor = 0.9659 Tooth Flux Dens = 1.7235T; Back Iron Dens =1.2311mH; Slots/pole/phase = 2.0000
Rotor Parameters: Magnet Height = 20 mm; Magnet Angle = 50 degm Air gap = 2.0000 mm ; Pole Pairs = 3.0000 Magnet Remanence = 1.2 T ; Air Gap Bg = 0.8617mH Magnet Factor = 1.3234; Skew Factor = 0.9886
Machine Losses: Core Loss = 1.5315kw; Armature Loss = 0.0444kw Windage Loss = 0.2469kw; Rotor Loss = TBD kw
Machine Weights: Core = 0.5430kg; Shaft = 0.1699kg Magnet = 0.2968kg Armature = 0.6708kg Services = 0.2521kg Total = 1.9326kg

Table 4: Rotor Losses Caused by Harmonics

Time Harmonic Losses = 0.4761 kw Space Harmonic Losses = 0.0290 kw Total Losses = 0.5052 kw

Magnet Loss = 0.0796 kW; THD = 10.2137

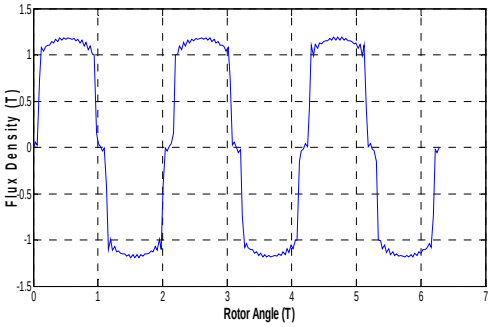

Fig. 10: Flux Density for 50 kW, Max. Eff.

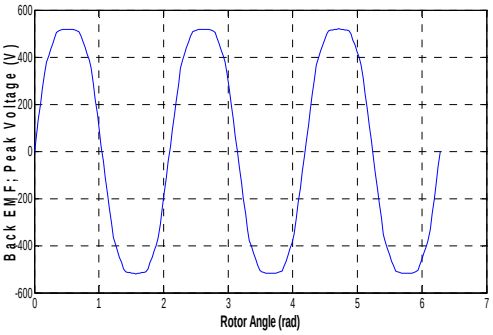

Fig. 11: EMF Waveform for 50 kW, Max. Eff.

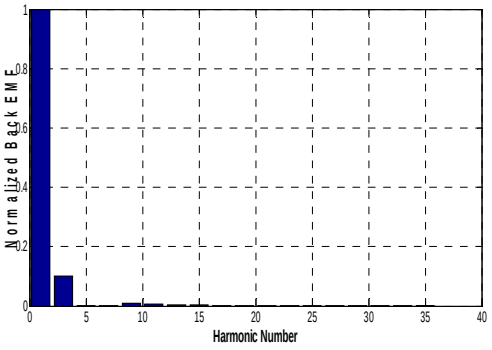

Fig. 12: Harm. Cont. 10.2137%; 50 kW, Max. Eff.

7. POLES NUMBER EFFECT ON SIZING PARAMETERS & M/C CHARACTERISTICS

This section illustrates the effect of poles number on some sizing parameters and motor characteristics. This is done at constant number of slots and phases. We take the previous case at 50 kW output power with tip speeds of 250, 200, 150, and 100m/s. The checked number of poles here are 4, 6, and 12 (Number of pole pairs: 2, 3, 6), i.e. one case before our selected value and one after.

The number of poles affects the electrical, magnetic, and structural performance, including the electrical frequency, the voltage waveforms, the magnetic flux; the magnetic volume; the air gap size, and the stator back iron thickness.

In general, if rotational speed is held constant as the number of poles increases:

- Number of slots/pole/phase changes affecting the output waveforms and THD.
- The weight of the machine decreases.
- The electrical frequency increases.

The following figures depict these various effects at 50 kW:

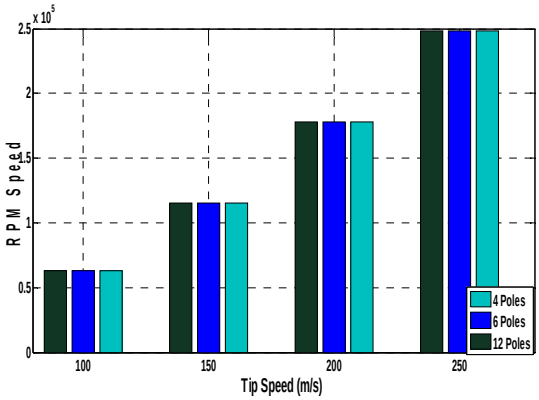

Fig. 13: RPM Speed with Tip Speed ;Pole Number.

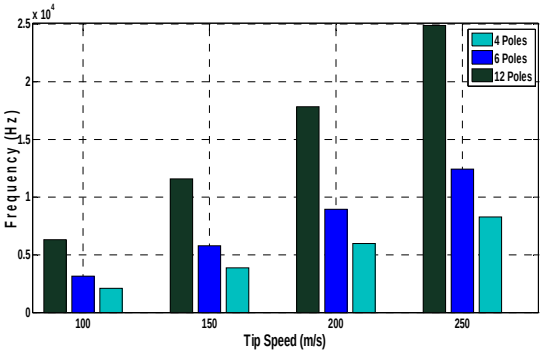

Fig. 14: Frequency with Tip Speed; Pole Number.

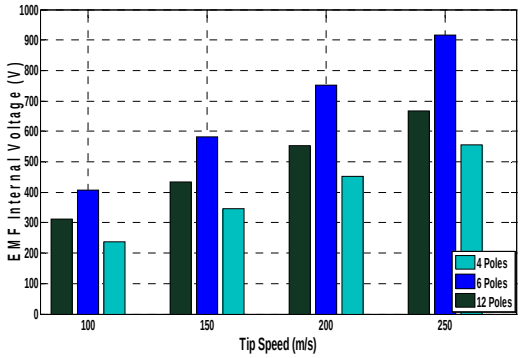

Fig.15: EMF with Tip Speed for Pole Number.

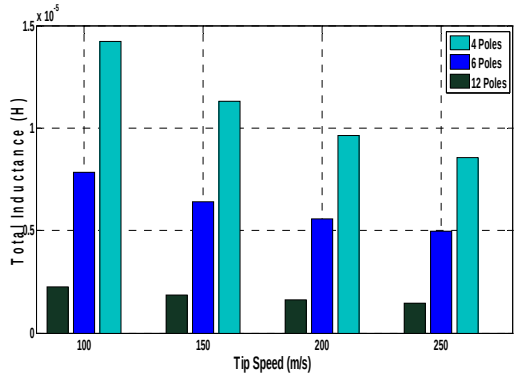

Fig.16: Inductance with Tip Speed; Pole Number.

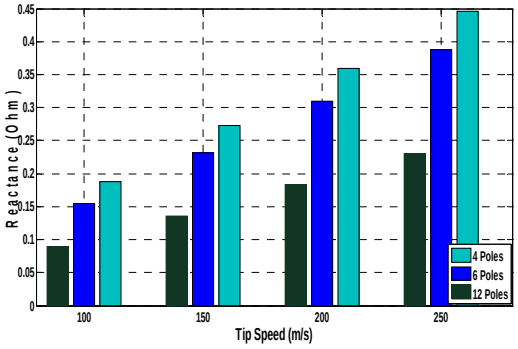

Fig. 17: Reactance with Tip Speed; Pole Number.

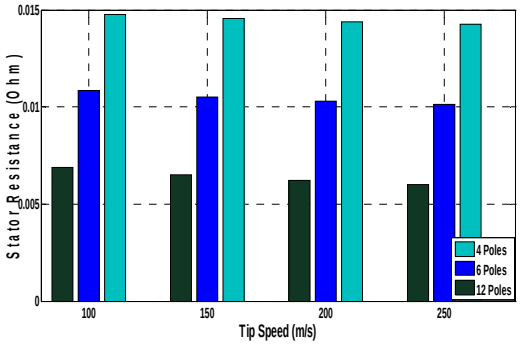

Fig. 18: Resistance with Tip Speed; Pole Number.

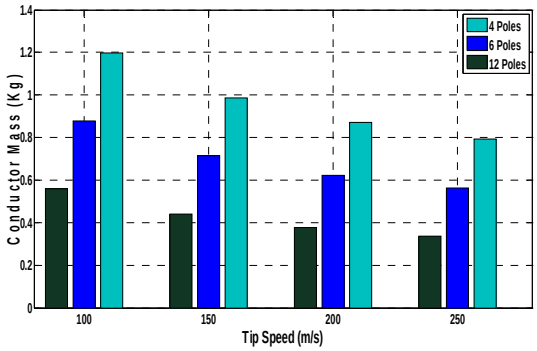

Fig.19: Conductor Mass with Tip Speed; Poles.

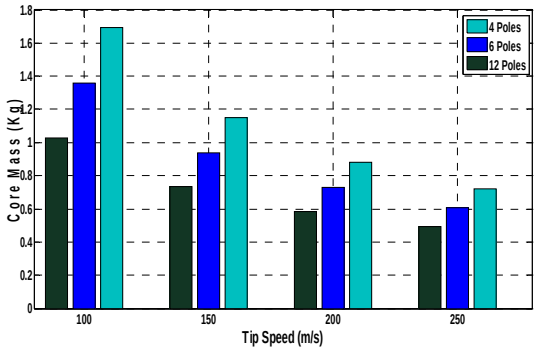

Fig. 20: Core Mass with Tip Speed; Pole Number.

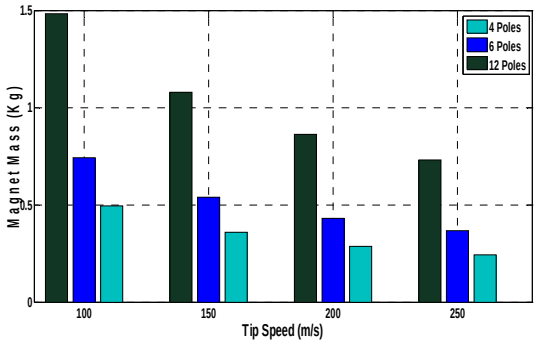

Fig. 21: Magnet Mass with Tip Speed; Poles. .

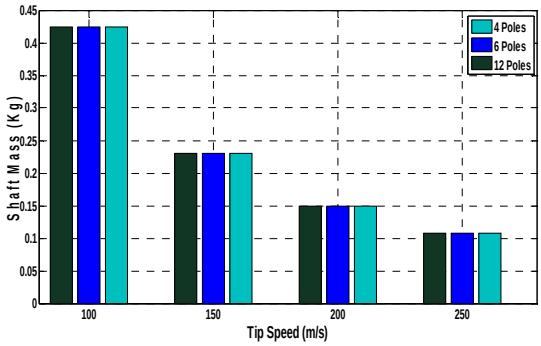

Fig. 22: Shaft Mass with Tip Speed; Pole Number.

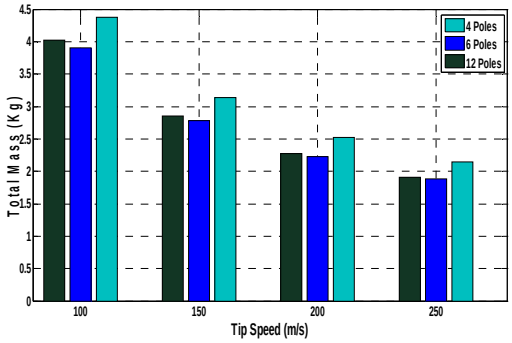

Fig. 23: Total Mass with Tip Speed; Pole Number.

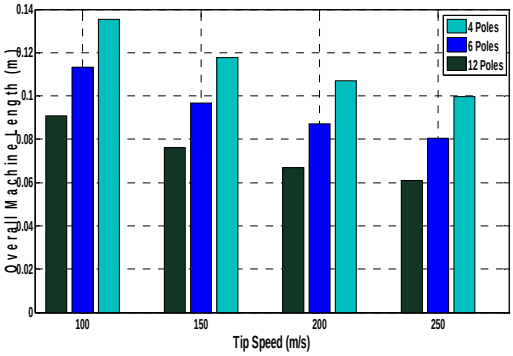

Fig. 24: Machine Length with Tip Speed; Poles.

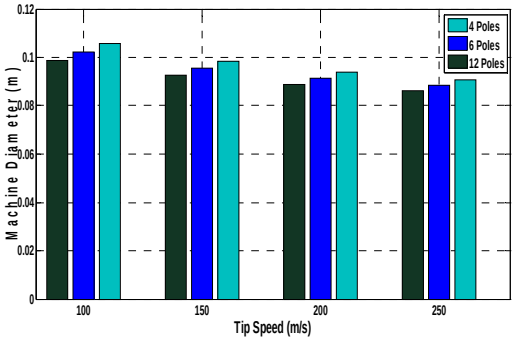

Fig. 25: Machine Diameter with Tip Speed; Poles.

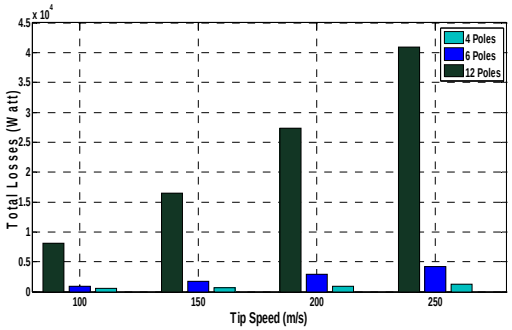

Fig. 26: Total Losses with Tip Speed; Pole Number.

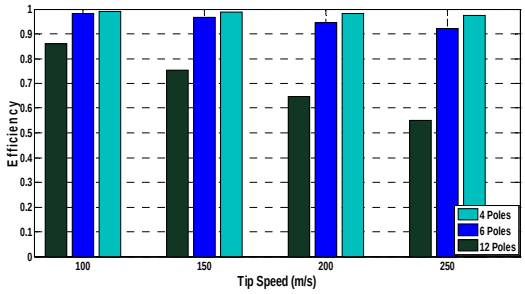

Fig.27 Efficiency with Tip Speed; Pole Number.

Finally, we have to return to the main case here at output power 50 kW and 250 m/s tip speed, to show the effect of varying the number of poles on the waveforms. This is done with poles number of 4 and 12. But at the first the magnet loss, rotor losses, and total harmonic distortion (THD) comparisons are presented in the form of charts. Then the flux density and EMF waveforms are introduced.

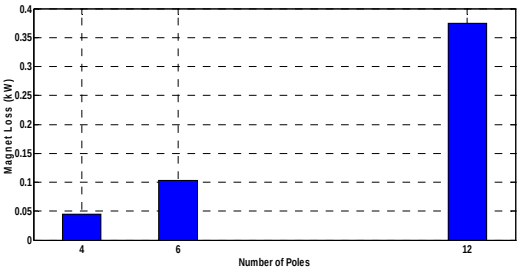

Fig.28: Magnet Loss with Pole Numbers.

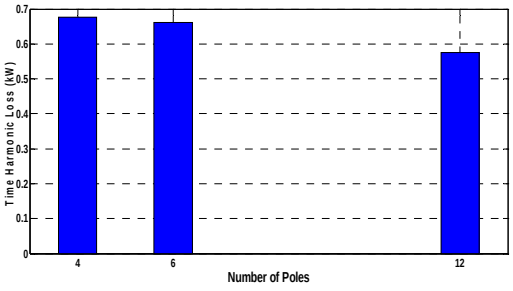

Fig.29: Time Harmonic Loss with Poles..

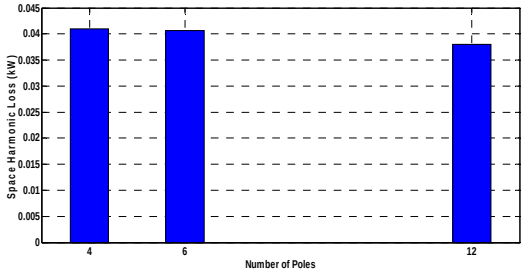

Fig. 30: Space Harmonic Loss with Poles.

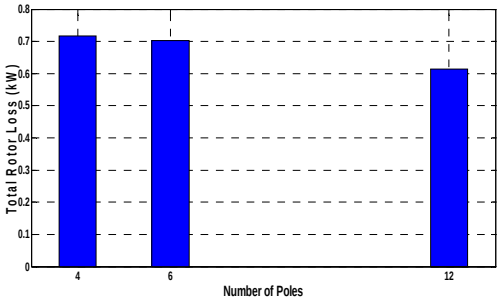

Fig. 31: Total Rotor Loss with Pole Numbers.

1) Waveforms at 50 kW, 250 m/s and 4 poles

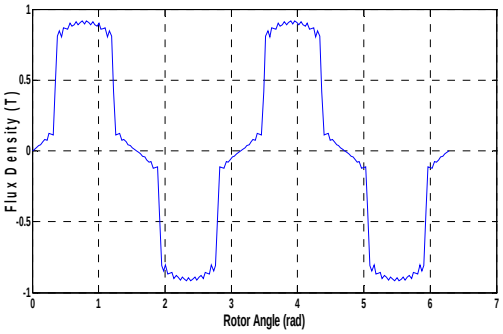

Fig. 32: Flux Density; 50 kW, 250 m/s and 4 poles.

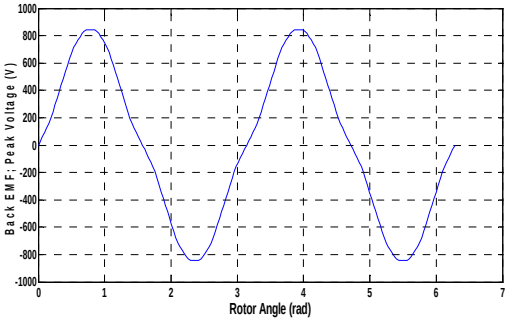

Fig. 33: EMF; 50 kW, 250 m/s and 4 poles.

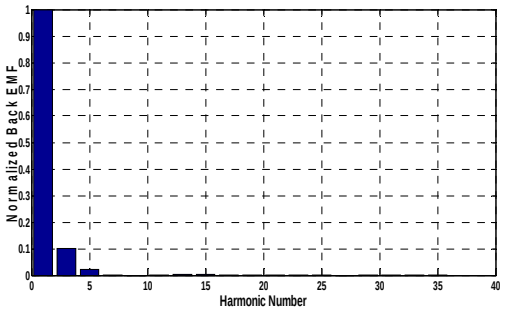

Fig. 34: Harmonic Content (10.2999%) for 50 kW, 250 m/s and 4 poles.

2) Waveforms at 50 kW, 250 m/s and 12 poles

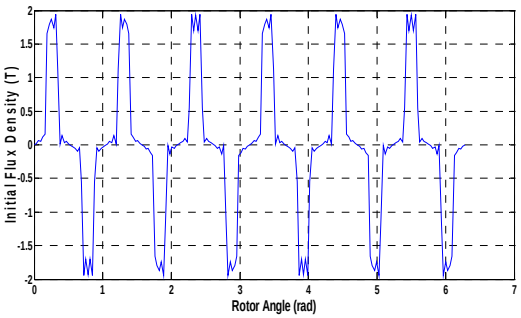

Fig. 35: Flux Den.; 50 kW, 250 m/s and 12 poles.

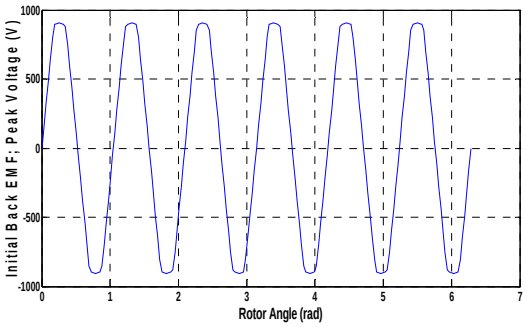

Fig. 36: EMF; 50 kW, 250 m/s and 12 poles.

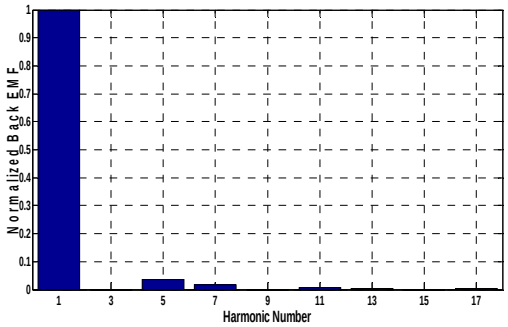

Fig. 37: Harmonic Content (3.9782%) for 50 kW, 250 m/s and 12 poles.

8. CONCLUSIONS

Due to the importance of High Speed PM Synchronous Motor especially is Spacecraft, and Aircraft applications; we propose 50 kW output power with 250 m/s tip speed. The sizing method presented gives a step by step classical method for high speed PM motor design. This is done at the first to present 1st trial and the second design trial is for maximum efficiency genetic one. Both trials are simulated using MATLAB and Genetic Algorithm Toolbox. The optimizing variables are rotor length to diameter ratio, rotor radius, and stack length, for the function, in constrained optimization genetic algorithm. Also, this paper affirms on the benefits of HSPM motors, compared to the original PM synchronous motors, since it offers significant reductions in both weights and volumes. It discusses the electrical and magnetic sizing of HSPMMs, at 50 kW power and tip speed of 250 m/s. In our study, we have found that a noticeable improvement appears in the performance parameters. The two design trials comparisons are introduced in analytical forms with study of machines waveforms, Total Harmonic Distortion (THD) and rotor losses. Finally, the effect of poles number on various sizing parameters and motor characteristics are illustrated in the form of charts with the waveforms. This is done at constant number of slots and phases with number of poles are 4, 6, and 12 at 50 kW output power and tip speeds of 250, 200, 150, and 100m/s. It should be notified that, for all cases, the constraints are generally the acceptable prescribed stress value, and the current density limitations. Moreover, some extra constraints for the optimizing variables in genetic case are taken into our considerations in the form of bounds.

REFRENCES:

[1] Ali Keyhani, Mohammad N. Marwali, and Min Dai, "Integration of Green and Renewable Energy in Electric Power Systems," Wiley, January 2010

[2] A. El Shahat, “Generating Basic Sizing Design Regression Neural Function for HSPMSM in Aircraft” EP-127, 13th International Conference on Aerospace Science & Aviation Technology, May 26 – 28, 2009, ASAT 2009 – Military Technical College, Cairo, Egypt.

[3] Adel El Shahat, and Hamed El Shewy, “High Speed PM Synchronous Motor Basic Sizing Neural Regression Function for Renewable Energy Applications”, Paper ID: X304, Accepted in 2nd International Conference on Computer and Electrical Engineering (ICCEE 2009); Dubai, UAE, December 28 - 30, 2009.

[4] Ahmad, R. A., Pan, Z., and Saban, D. M., "On-Board Electrical Network Topology Using High Speed Permanent Magnet Generators," Electric Ship Technologies Symposium, 2007. ESTS apos;07. IEEE Volume , Issue , 21-23, pp.356 – 362, May 2007.

[5] Scridon, S., Boldea, I., Tutelea, Blaabjerg, L., F., and Ritchie, E., "BEGA – A Biaxial Excitation Generator for Automobiles: Comprehensive Characterization and Test Results," IAS, 2004, Industry Applications Conference, 2004. 39th IAS Annual Meeting Conference Record of the 2004 IEEE, vol.3, pp. 1682 – 1690, 3-7 Oct. 2004.

[6] Binder, A., Schneider, T., and Klohr, M., "Fixation of Buried and Surface- Mounted Magnets in High-Speed Permanent-Magnet Synchronous Machines," IEEE Trans. On Industry Applications, Vol. 42, NO. 4, pp. 1031 – 1037, July/August, 2006.

[7] Hosseini, S. M., Mirsalim, M. A., and Mirzaei, M. , "Design, Prototyping, and Analysis of a Low Cost Axial-Flux Coreless Permanent-Magnet Generator," IEEE Trans. On Magnet., Vol. 44, No. 1, pp. 75 – 80, Jan. 2008.

[8] Mellor, P.H., Burrow, S.G., Sawata, T., and Holme, M., "A Wide – Speed – Range Hybrid Variable – Reluctance / Permanent – Magnet Generator for Future Embedded Aircraft Generation Systems," IEEE Trans. On Industry Applications, Vol. 41, No. 2, PP. 551 – 556, March/April 2005.

[9] Sadeghierad, M., Lesani, H., Monsef, H., and Darabi, A., "Design considerations of High Speed Axial Flux permanent magnet Generator with Coreless Stator," The 8th International Power Engineering Conference (IPEC), pp. 1098 – 1102, 2007.

[10] Arnold, D. P., Das, S., Park, J. W., Zana, I., Lang, J. H., and Allen, M. G., "Micro fabricated High-Speed Axial-Flux Multi watt Permanent- Magnet Generators—Part II: Design, Fabrication, and Testing," Journal Of Micro Electromechanical Systems, Vol. 5, No. 5, pp. 1351 – 1363, October 2006.

[11] Paulides, J. J. H., Jewell, G. W., and Howe, D., "An Evaluation of Alternative Stator Lamination Materials for a High – Speed, 1.5 MW, Permanent Magnet Generator," IEEE

Trans. On Magnetics, Vol. 40, No. 4, pp. 2041 - 2043, July 2004.

[12] Jang, S. M., Cho, H. W., and Jeong, Y. H., "Influence on the rectifiers of rotor losses in high – speed permanent magnet synchronous alternator," Journal of Applied Physics, 08R315, American Institute of Physics, 08R315-1 – 08R315-3, 2006.

[13] Kolondzovski, Z., "Determination of critical thermal operations for High – speed permanent magnet electrical machines," The International Journal for Computation and Mathematics in Electrical and Electronic Engineering, Vol. 27 No. 4, pp. 720-727, 2008.

[14] Nagorny, A. S., Dravid, N. V., Jansen, R. H., and Kenny, B. H., "Design Aspects of a High Speed Permanent Magnet Synchronous Motor / Generator for Flywheel Applications," NASA/TM—2005-213651 June 2005, International Electric Machines and Drives Conference sponsored by the IEEE Industry Applications Society, IEEE Power Electronics Society, IEEE Power Engineering Society, and IEEE Industrial Electronics Society, San Antonio, Texas, May 15–18, 2005.

[15] Hanselmann, D. C., Brushless Permanent Magnet Motor Design, New York: McGraw-Hill, 1994.

[16] Hendershot, J. R. and Miller, T. J. E., Design of Brushless Permanent Magnet Motors, Oxford, U.K.: Magna Physics Publishing and Clarendon Press, 1994.

[17] Rucker, J. E., Kirtley, J. L., McCoy, Jr. T. J., "Design and Analysis of a Permanent Magnet Generator For Naval Applications," IEEE Electric Ship Technologies Symposium, pp. 451 – 458, 2005.

[18] Kang, D., Curiac, P., Jung, Y., and Jung, S., "Prospects for magnetization of large PM rotors: conclusions from a development case study," IEEE trans. On Energy Conversion, vol. 18, no. 3, Sept. 2003.

[19] Paulides, J., Jewell, G., and Howe, D., "An evaluation of alternative stator lamination materials for a high speed, 1.5 MW, permanent Magnet Generator," IEEE Trans. On Magnetics, vol. 40, no. 4, July 2004.

[20] Bianchi, N., and Lorenzoni, A., "Permanent magnet generators for wind power industry: an overall comparison with traditional generators," Opportunities and advances in international power generation, conference publication No. 419, 1996.

[21] Rahman, M. A., and Slemon, G. R., "Promising Applications of Neodymium Iron Boron Iron Magnets in Electrical Machines," IEEE Trans. On Magnetics, Vol. No. 5, Sept 1985.

[22] Polinder, H. and Hoeijmakers, M. J., "Eddy – Current Losses in the Segmented Surface Mounted Magnets of a PM Machine," IEE Proceedings, Electrical Power Applications, Vol. 146, No. 3, May 1999.

[23] Aglen, O., and Andersson, A., "Thermal Analysis of a High Speed Generator," Industry Applications Conference, 38th IAS Annual Meeting. Con. vol.1, pp. 547- 554, 12-16 Oct. 2003. Current Version Published: 2004-01-07 IEEE Transactions, 2003.

[24] Pepi, J., and Mongeau, P., "High power density permanent magnet generators," DRS Electric power technologies, Inc., 2004.

[25] Kong X., Wang F., and Sun Y. (2007) 'Comparison of High Speed PM Generator with PM Doubly Fed Reluctance Generator for Distributed Power Generation System', 2nd IEEE Conference on Industrial Electronics and Applications, 2007. ICIEA 2007, pp. 1193 – 1197.

[26] I. Boldea and S. A. Nasar, Induction Machine Handbook, CRC Press, Boca Raton, Fl, 2001.

[27] B. Amin, "Contribution to iron-loss evaluation in electrical machines", European Trans. on Elect. Power Eng., vol. 5, 1995, pp. 325-332.

[28] Z.Q. Zhu, D. Howe, E. Bolte, B. Ackermann, "Instantaneous Magnetic Field distribution in brushless permanent-magnet dc motors, part I: open-circuit field", IEEE Trans. on Magnetics, vol. 29, 1993, pp. 124-135.

[29] Z.Q. Zhu, D. Howe, "Instantaneous Magnetic Field distribution in brushless permanent-magnet dc motors, part II: armature-reaction field", IEEE Trans. on Magnetics, vol. 29, 1993, pp. 136-142.

[30] Z.Q. Zhu, D. Howe, "Instantaneous Magnetic Field distribution in brushless permanent-magnet dc motors, part III: effect of stator slotting", IEEE Trans. on Magnetics, vol. 29, 1993, pp. 143-151.

[31] Z.Q. Zhu, D. Howe, "Instantaneous Magnetic Field distribution in brushless permanent-magnet dc motors, part IV: magnetic field on load", IEEE Trans. on Magnetics, vol. 29, 1993, pp. 152-158.

[32] J.G. Zhu, S.Y.R. Hui, V.S. Ramsden, "Discrete modelling of magnetic cores including

hysteresis, eddy current, and anomalous losses", IEE Proc., Part A, Sc., Measure. and Tech., vol. 140, 1993, pp. 317-322.

[33] I. Boldea, Variable speed electric generators, CRC Press, Florida, 2006.

[34] J.G. Zhu, S.Y.R. Hui, V.S. Ramsden, "A generalized dynamic circuit model of magnetic cores for low- and high-frequency applications - Part I: Theoretical calculation of the equivalent core loss resistance", IEEE Trans. Power Elect., vol. 11, 1996, pp.246-250.

[35] Moré, J.J. and Sorensen D.C. "Computing a Trust Region Step", SIAM Journal on Scientific and Statistical Computing, Vol. 3, 1983, pp 553-572.

[36] Zhang, Y. "Solving Large-Scale Linear Programs by Interior-Point Methods Under the

[37] MATLAB Environment", Department of Mathematics and Statistics, University of Maryland, Baltimore County, Baltimore, MD, Technical Report TR96-01, 1995.

[38] Pepi, J. and Mongeau, P. , High power density permanent magnet generators, DRS Electric power technologies, Inc, 2004.

[39] Conn, A. R., Gould N. I. M., and Toint Ph. L. (1991) 'A Globally Convergent Augmented Lagrangian Algorithm for Optimization with General Constraints and Simple Bounds', SIAM Journal on Numerical Analysis, Volume 28, Number 2, pages 545–572.

[40] Conn, A. R., Gould N. I. M., and Toint Ph. L. (1997) 'A Globally Convergent Augmented Lagrangian Barrier Algorithm for Optimization with General Inequality Constraints and Simple Bounds', Mathematics of Computation, Volume 66, Number 217, pages 261–288.

[41] I. H. Shames, and J. M. Pitarresi, Introduction to Solid Mechanics, 3rd Ed., Prentice Hall, 2000.

[42] M. F. Ashby, and D. R. H. Jones, Engineering Materials, Pergamon Press, 1991.

[43] J. L. Kirtley, and E. C. Lovelace, "Drag Loss in Retaining Rings of Permanent Magnet Motors," SatCon Technology Corporation, March, 2003.

[44] H. Polinder and M. J. Hoeijmakers, "Eddy-Current Losses in the Permanent Magnets of a PM Machine," EMD 97, Conference Publication No. 444, 1997.